

PHASE TRANSFORMATION AND GROWTH OF HYGROSCOPIC AEROSOLS

I. N. Tang
Environmental Chemistry Division
Department of Applied Science
Brookhaven National Laboratory
Upton, NY 11973-5000

November 1999
[Original Manuscript Date: September 1995]

Published in
Aerosol Chemical Processes in the Environment,
Chapter 4, Spurny, K. R. and Hochrainer, D., Ed., pp. 61-80,
CRC Press LLC, Boca Raton, 2000.

By acceptance of this article, the publisher and/or recipient acknowledges the U.S. Government's right to retain a nonexclusive, royalty-free license in and to any copyright covering this paper.

This research was performed under the auspices of the U.S. Department of Energy under Contract No. DE-AC02-98CH10886.

4 Phase Transformation and Growth of Hygroscopic Aerosols

Ignatius N. Tang

CONTENTS

Introduction	
Single-Particle Levitation Experiments	
Hydration Behavior and Metastability	
Droplet Equilibrium Size and Water Activity	
Particle Deliquescence	
Solute Nucleation and Droplet Efflorescence	
References	

INTRODUCTION

Ambient aerosols play an important role in many atmospheric processes affecting air quality, visibility degradation, and climatic changes as well. Both natural and anthropogenic sources contribute to the formation of ambient aerosols, which are composed mostly of sulfates, nitrates, and chlorides in either pure or mixed forms. These inorganic salt aerosols are hygroscopic by nature and exhibit the properties of deliquescence and efflorescence in humid air. For pure inorganic salt particles with diameter larger than 0.1 micron, the phase transformation from a solid particle to a saline droplet occurs only when the relative humidity in the surrounding atmosphere reaches a certain critical level corresponding to the water activity of the saturated solution. The droplet size or mass in equilibrium with relative humidity can be calculated in a straightforward manner from thermodynamic considerations. For aqueous droplets 0.1 micron or smaller, the surface curvature effect on vapor pressure becomes important and the Kelvin equation must be used.¹

In reality, however, the chemical composition of atmospheric aerosols is highly complex and often varies with time and location. Junge² has shown that the growth of atmospheric aerosol particles in continental air masses deviates substantially from what is predicted for the growth of pure salts. He explained this difference by assuming a mixture of soluble and insoluble materials within the particle, thus introducing the concept of mixed nuclei for atmospheric aerosols. Subsequent investigation by Winkler³ led to an empirical expression for the growth of continental atmospheric aerosol particles. Tang⁴ considered the deliquescence and growth of mixed-salt particles, relating aerosol phase transformation and growth to the solubility diagrams for multicomponent electrolyte solutions.

In this chapter, an exposition of the underlying thermodynamic principles on aerosol phase transformation and growth is given. Recent advances in experimental methods utilizing single-particle levitation are discussed. In addition, pertinent and available thermodynamic data, which are needed for predicting the deliquescence properties of single- and multicomponent aerosols, are compiled. Information on the composition and temperature dependence of these properties is required in mathematical models for describing the dynamic and transport behavior of ambient

aerosols. Such data, however, are very scarce in the literature, especially when dealing with aerosols composed of mixed salts as an internal mixture.

SINGLE-PARTICLE LEVITATION EXPERIMENTS

Numerous methods have been employed by investigators to study aerosol phase transition and growth in humid air. Thus, Dessens⁵ and Twomey⁶ conducted deliquescence experiments with both artificial salt and ambient particles collected on stretched spider webs. They examined the particles with a microscope and noted phase transition in humid air. Orr et al.⁷ investigated the gain and loss of water with humidity change by measuring the change in electrical mobility for particles smaller than 0.1 μm . Winkler and Junge⁸ used a quartz microbalance and studied the growth of both artificial inorganic salt aerosols and atmospheric aerosol samples collected on the balance by impaction. Covert et al.⁹ also reported aerosol growth measurements using nephelometry. Finally, Tang¹⁰ constructed a flow reactor with controlled temperature and humidity and measured the particle size changes of a monodisperse aerosol with an optical counter. Although these methods suffer from either possible substrate effects or some difficulties in accurate particle size and relative humidity measurements, they have provided information for a clear understanding of the hydration behavior of hygroscopic aerosols.

In recent years, however, new experimental techniques have been developed for trapping a single micron-sized particle in a stable optical or electrical potential well. These new techniques have made it possible to study many physical and chemical properties that are either unique to small particles or otherwise inaccessible to measurement with bulk samples. An earlier review by Davis¹¹ documented the progress up to 1982. Since then, many interesting investigations have appeared in the literature. In particular, thermodynamics^{12,14} and optical properties^{15,16} of electrolyte solutions at concentrations far beyond saturation that could not have been achieved in the bulk, can now be measured with a levitated microdroplet. This is accomplished by continuously and simultaneously monitoring the changes in weight and in Mie scattering patterns of a single suspended solution droplet undergoing controlled growth or evaporation in a humidified atmosphere, thereby providing extensive data over the entire concentration region. Other interesting works on the physics and chemistry of microparticles have been discussed in the recent review by Davis.¹⁷ In this section, the experimental methods used by Richardson and Kurtz¹⁸ and Tang et al.¹³ are described in some detail.

Single particle levitation is achieved in an electrodynamic balance (or quadrupole cell), whose design and operating principles have been described elsewhere.¹⁹⁻²² Briefly, an electrostatically charged particle is trapped at the null point, of the cell by an ac field imposed on a ring electrode surrounding the particle. The particle is balanced against gravity by a dc potential, U , established between two endcap electrodes positioned symmetrically above and below the particle. All electrode surfaces are hyperboloidal in shape and separated by Teflon insulators. When balanced at the null point, the particle mass, w is given by

$$w = \frac{qU}{gz_o}, \quad (4.1)$$

where q is the number of electrostatic charges carried by the particle, g the gravitational constant, and z_o the characteristic dimension of the cell. It follows that the relative mass changes, w/w_o , resulting from water vapor condensation or evaporation can be measured as precisely as measurement of the dc voltage changes, U/U_o , that are necessary for restoring the particle to the null point. Here, the subscript, o , refers to measurements for the initial dry salt particle.

A schematic diagram of the apparatus is shown in Figure 4.1. The single-particle levitation cell is placed inside a vacuum chamber equipped with a water jacket that can maintain the cell

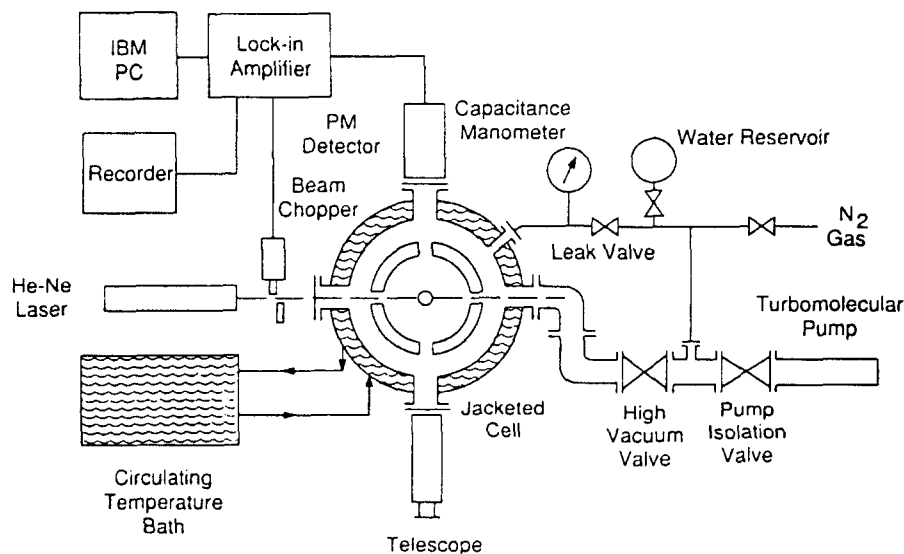


FIGURE 4.1 Schematic diagram of the single-particle levitation apparatus.

temperature within $\pm 0.1^\circ\text{C}$. A linear, vertically polarized He-Ne laser beam, entering the cell through a side window, illuminates the particle, 6 to 8 μm in diameter when dry. The particle position is continuously monitored by a CCD video camera and displayed on a TV screen for precise null point balance. The 90° scattered light is also continuously monitored with a photomultiplier tube. The laser beam, which is mechanically chopped at a fixed frequency, is focused on the particle so that a lock-in amplifier can be used to achieve high signal-to-noise ratios in the Mie scattering measurement.

Initially, a filtered solution of known composition is loaded in a particle gun; a charged particle is injected into the cell and captured in dry N_2 at the center of the cell by properly manipulating the ac and dc voltages applied to the electrodes. The system is closed and evacuated to a pressure below 10^{-7} torr. The vacuum is then valved off and the dc voltage required to position the particle at the null point is now noted as U_0 . The system is then slowly back filled with water vapor during particle deliquescence and growth. Conversely, the system is gradually evacuated during droplet evaporation and efflorescence. The water vapor pressure, p_1 , and the balancing dc voltage, U , are simultaneously recorded in pairs during the entire experiment. Thus, the ratio, U_0/U , represents the solute mass fraction and the ratio, p_1/p_1^0 , gives the corresponding water activity, a_1 , at that point. Here, p_1^0 is the vapor pressure of water at the system temperature. The measurement can be repeated several times with the same particle by simply raising the water vapor pressure again and repeating the cycle. The reproducibility is better than $\pm 2\%$.

HYDRATION BEHAVIOR AND METASTABILITY

A deliquescent salt particle, such as KCl, NaCl, or a mixture of both, exhibits characteristic hydration behavior in humid air. Typical growth and evaporation cycles at 25°C are shown in Figure 4.2. Here, the particle mass change resulting from water vapor condensation or evaporation is plotted as a function of relative humidity (RH). Thus, as RH increases, a crystalline KCl particle (as illustrated by solid curves) remains unchanged (curve A) until RH reaches its deliquescence point (RHD) at 84.3% RH. Then, it deliquesces spontaneously (curve B) to form a saturated solution droplet by water vapor condensation, gaining about 3.8 times its original weight. The droplet continues to grow as RH further increases (curve C). Upon decreasing RH, the solution droplet loses weight by water evaporation. It remains a solution droplet even beyond its saturation point

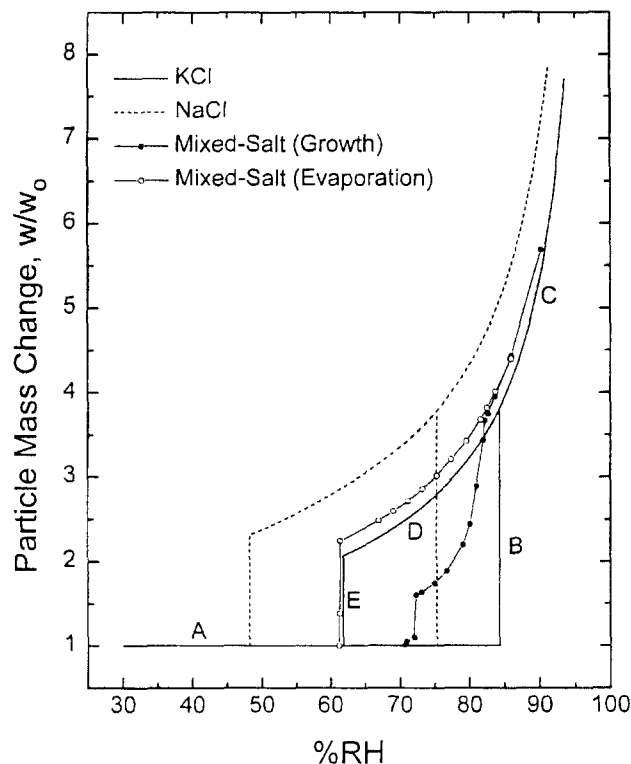


FIGURE 4.2 Growth and evaporation of KCl/NaCl particles in humid environment at 25°C.

and becomes highly supersaturated as a metastable droplet (curve D) at RH much lower than RHD. Finally, efflorescence occurs at about 62% RH (curve E), when the droplet suddenly sheds all its water content and becomes a solid particle. Similar behavior is illustrated in Figure 4.2 as dashed curves for an NaCl particle, which deliquesces at 75.4% at 75.4% RH and crystallizes at about 48% RH. Note that, for a single-salt particle, the particle is either a solid or a droplet, but not in a state of partial dissolution.

In a bulk solution, crystallization always takes place not far beyond the saturation point. This happens because the presence of dust particles and the container walls invariably induce heterogeneous nucleation at a much earlier stage than what would be expected for homogeneous nucleation to occur. On the other hand, in a solution droplet where the presence of an impurity nucleus is rare, homogeneous nucleation normally proceeds at high supersaturations. Thus, the hysteresis shown in Figure 4.2 by either the KCl or NaCl particle represents a typical behavior exhibited by all hygroscopic aerosol particles. The observations reported by Rood et al.²³ also revealed that in both urban and rural atmospheres, metastable droplets indeed existed more than 50% of the time when the RH was between about 45 and 75%. Since solution droplets tend to become highly supersaturated before efflorescence, the resulting solid may be in a metastable state that is not predicted from the bulk-phase thermodynamic equilibrium. In fact, some solid metastable states formed in hygroscopic particles may not even exist in the bulk phase.²⁴ It follows that the hydration properties of hygroscopic aerosol particles cannot always be predicted from their bulk solution properties.

A case of interest is Na_2SO_4 aerosol particles. In bulk solutions at temperatures below 35°C, sodium sulfate crystallizes with ten water molecules to form the stable solid-phase decahydrate, $\text{Na}_2\text{SO}_4 \cdot 10\text{H}_2\text{O}$.²⁵ In suspended microparticles, however, it is the anhydrous solid, Na_2SO_4 , that is formed most frequently from the crystallization of supersaturated solution droplets. This fact is

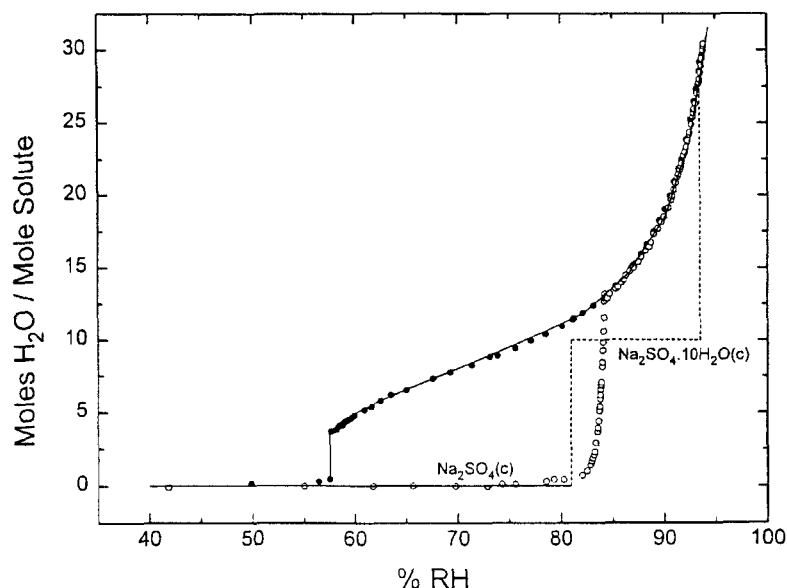
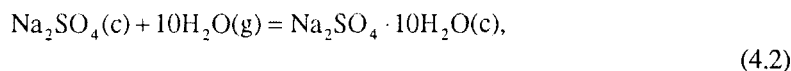


FIGURE 4.3 Growth and evaporation of a Na_2SO_4 particle in humid environment at 25°C .

established both by particle mass measurements¹⁴ and by Raman spectroscopy.²⁴ Figure 4.3 shows the growth (open circles) and evaporation (filled circles) of an Na_2SO_4 particle in a humid environment at 25°C . The hydration behavior is qualitatively very similar to that of the KCl or NaCl particle shown in Figure 4.2. Thus, as the RH increases, an anhydrous Na_2SO_4 particle deliquesces at 84% RH to form a saturated solution droplet containing about 13 moles H_2O per mole solute (moles H_2O /mole solute). Upon evaporation, the solution droplet becomes highly supersaturated until, finally, crystallization occurs at about 58% RH, yielding an anhydrous particle.

At high supersaturations, the decahydrate is no longer the most stable state. The relative stability between anhydrous Na_2SO_4 and the decahydrate can be estimated from a consideration of the standard Gibb's free energy change, ΔG° , of the system:

so that,



$$\Delta G^\circ = \Delta G_f^\circ[\text{Na}_2\text{SO}_4 \cdot 10\text{H}_2\text{O}] - \Delta G_f^\circ[\text{Na}_2\text{SO}_4] - 10\Delta G_f^\circ[\text{H}_2\text{O}] = -RT \ln(1/p_1^{10}).$$

Here, *c* and *g* in the parentheses refer to the crystalline state and gas phase, respectively. Taking the tabulated²⁶ ΔG_f° values -871.75 , -303.59 , and -54.635 kcal mol⁻¹ for $\text{Na}_2\text{SO}_4 \cdot 10\text{H}_2\text{O}(c)$, $\text{Na}_2\text{SO}_4(c)$, and $\text{H}_2\text{O}(g)$, respectively, we obtain a value of -21.81 kcal mol⁻¹ for ΔG° , which leads to 19.2 torr as the equilibrium partial pressure of water vapor, or 81% RH at 25°C . It follows that, instead of the decahydrate, the anhydrous Na_2SO_4 becomes the most stable state below 81% RH. Thus, as depicted by the dashed lines shown in Figure 4.3, a solid anhydrous Na_2SO_4 particle would have transformed into a crystalline decahydrate particle at 81% RH, which would then deliquesce at 93.6% RH, to become a saturated solution droplet containing about 38 moles H_2O /mole solute, according to solution thermodynamics.²⁷ However, the observed hydration behavior of the particle, as shown in Figure 4.3, is quite different from what is predicted from bulk-phase thermodynamics.

The hydration behavior of a mixed-salt particle is more complicated in that partially dissolved states may be present. This is illustrated again in Figure 4.2 by the growth (filled circles) and

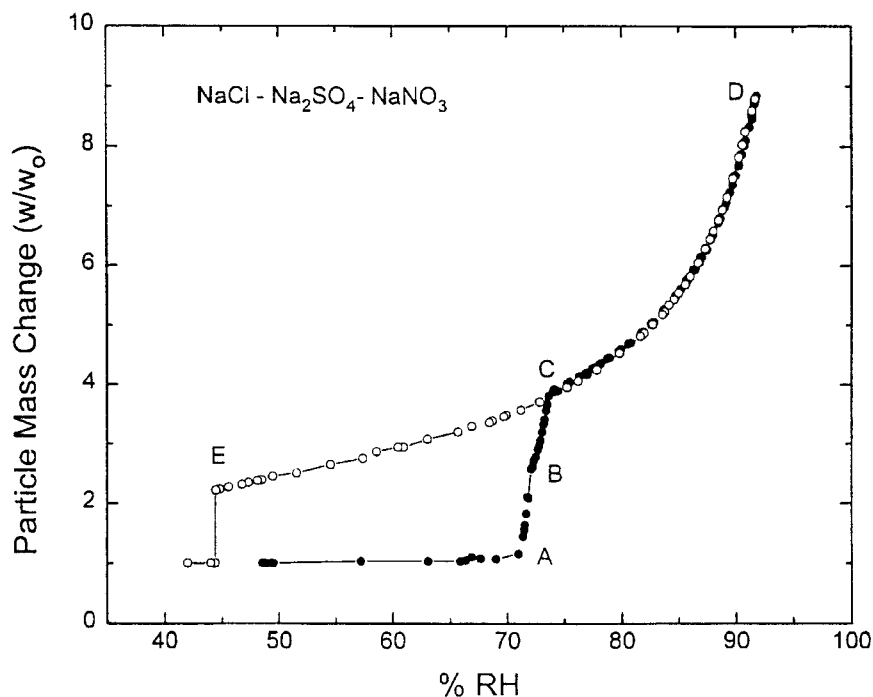


FIGURE 4.4 Growth and evaporation of a mixed-salt particle composed of NaCl, Na₂SO₄, and NaNO₃ in humid environment at 17.5°C.

evaporation (open circles) of a mixed-salt particle composed of 80% KCl and 20% NaCl by weight. The particle was observed to deliquesce at 72.5% RH, followed by a region where excess KCl gradually dissolved in the solution as RH increased. The particle became a homogeneous solution droplet at 82% RH. Upon evaporation, the solution droplet was observed to crystallize at about 61% RH. Figure 4.4 shows the growth and evaporation of another mixed-salt particle composed of equal amounts of NaCl, Na₂SO₄, and NaNO₃. At 17.5°C, the particle was observed to deliquesce at 72% RH.^{16,28} There was also a region following deliquescence where excess solids were gradually dissolving in the solution. At 74% RH, this mixed-salt particle became a homogeneous solution droplet, which would then grow or evaporate as RH was increasing or decreasing, respectively, as shown in Figure 4.4. Upon evaporation, the particle was observed to persist as a metastable solution droplet and finally crystallized at about 45% RH. Thus, the general hydration characteristics are similar for multicomponent aerosol particles.

Tang⁴ has considered the phase transformation and droplet growth of mixed-salt aerosols. The particle deliquescence is determined by the water activity of the eutonic point, E, in the solubility diagram, as shown in Figure 4.5 for the KCl–NaCl–H₂O system. Here wt% NaCl is plotted vs. wt% KCl for ternary solutions containing the two salts as solutes and H₂O as the solvent. The solid curves, AE and BE, shown here for 25°C, are solubility curves constructed from data taken from Seidell and Linke.²⁵ Each point on the solubility curves determines the composition of a saturated solution in equilibrium with a specific water activity. Thus, point A represents the solubility of NaCl at a concentration of 26.42 wt% and a_1 of 0.753, and point B is the solubility of KCl at 26.37 wt% and a_1 of 0.843. The solution is saturated with NaCl along the curve AE and with KCl along BE. The eutonic point, E, is the composition (KCl/NaCl = 11.14/20.42%) where both salts have reached their solubility limits in the solution at the given temperature. This is usually the composition at which the water activity is the lowest among all compositions.^{4,29} It is, therefore, the composition of the solution droplet formed when a solid particle of any composition (e.g., KCl/NaCl

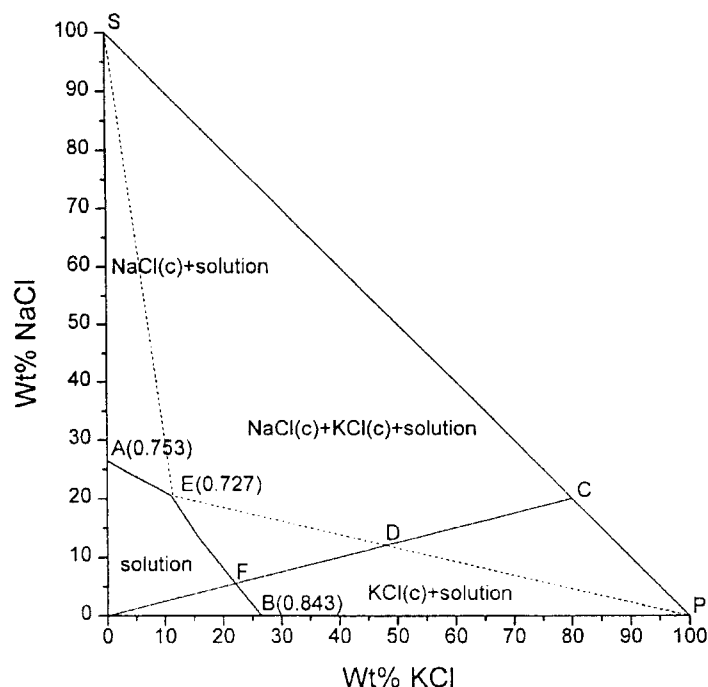


FIGURE 4.5 Solubility diagram for the system KCl-NaCl-H₂O at 25°C.

= 80/20%, as represented by point C) first deliquesces. Wexler and Seinfeld³⁰ have shown theoretically that the RHD of one electrolyte is lowered by the addition of a second electrolyte, essentially explaining why the RHD of a mixed-salt particle is lower than that of either single-salt particles.

EQUILIBRIUM DROPLET SIZE AND WATER ACTIVITY

The equilibrium between an aqueous salt solution droplet and water vapor in humid air at constant temperature and relative humidity has been considered by many investigators since the earlier work of Koehler.³¹ A thorough account of the thermodynamics of droplet-vapor equilibrium can be found in books by Dufour and Defay³² and by Pruppacher and Klett.³³ For a solution droplet containing nonvolatile solutes, the equation

$$\ln \frac{p_1}{p_1^0} = \ln \gamma_1 y_1 + \frac{2v_1 \sigma}{RT r} \quad (4.3)$$

is quite general and applies to both single and multicomponent systems, provided that the solution properties are determined for the system under consideration.^{4,34} Equation (4.3) relates the equilibrium radius r of a droplet of composition y_1 (mole fraction) to RH, namely, $\%RH = 100 p_1/p_1^0$, and to the solution properties such as the activity coefficient γ_1 , partial molar volume v_1 , and surface tension σ . Here, the subscript 1 refers to water as the solvent. p_1 is the partial pressure and p_1^0 the saturation vapor pressure of water at temperature T (°K). R is the gas constant. For a droplet 0.1 μm in diameter, the contribution of the second term on the right-hand side of Equation (4.3) is about 2%. Consequently, for larger droplets, the droplet composition agrees closely with that of a bulk solution in equilibrium with its water vapor at given T , and the water activity of the solution droplet is simply

$$a_1 = \gamma_1 y_1 = \frac{p_1}{p_1^0} = \frac{\%RH}{100}. \quad (4.4)$$

The change in particle size at a given relative humidity can readily be deduced from a material balance on salt content before and after droplet growth to its equilibrium size. The following equation is obtained:

$$\frac{d}{d_0} = \left(\frac{100p_0}{xp} \right)^{1/3} \quad (4.5)$$

Here, d and p are, respectively, the diameter and density of a droplet containing $x\%$ by weight of total salts. Again, the subscript, o , refers to the dry salt particle. It follows that, in order to calculate droplet growth as a function of RH, it is essential to have water activity and density data as a function of droplet composition.

The simplest measurements that can be made with the single-particle levitation technique are water activities of electrolyte solutions over a large concentrated range, especially at high supersaturations that could not have been done with bulk solutions. For highly hygroscopic inorganic salts such as NH_4HSO_4 , NaHSO_4 , and NaNO_3 , the solution droplets may persist in the liquid form to such a degree that one solvent molecule is shared by five or six solute molecules.¹⁶ Such data are not only required in modeling the hydration behavior of atmospheric aerosols, but also crucial to testing and furthering the development of solution theories for high concentrations and multi-component systems. Indeed, some efforts have begun to modify and extend Pitzer's semiempirical thermodynamic model for relatively dilute electrolyte solutions to high concentrations.³⁵⁻³⁷

$(\text{NH}_4)_2\text{SO}_4$ is one of the most important constituents of the ambient aerosol. A large effort has been made to obtain thermodynamic and optical data for modeling computations. Thus, Richardson and Spann¹² have made water activity measurements at room temperature with $(\text{NH}_4)_2\text{SO}_4$ solution droplets levitated in a chamber that can be evacuated and back-filled with water vapor. Cohen et al.¹⁴ have employed an electrodynamic balance placed in a continuously flowing gas stream at ambient pressures and made water activity measurements for a number of electrolytes, including $(\text{NH}_4)_2\text{SO}_4$. The two sets of data show some discrepancies, which amount to 0.04 to 0.05 in water activities, or 5 to 6 wt% at high concentrations. Chan et al.³⁸ have repeated the measurements in a spherical void electrodynamic levitator (SVEL) and obtained results consistent with those of Cohen et al. The SVEL is a variation of the electrodynamic balance with the inner surfaces of the electrodes designed to form a spherical void.³⁹ Tang and Munkelwitz¹⁶ have also made extensive measurements in their apparatus, which is closer in design to that of Richardson and Spann but better thermostatted. Their results, together with those of previous studies, are shown in Figure 4.6. It appears that, although the agreement among all data sets is acceptable for aerosol growth computations, there is a need for more intercomparison studies to reduce the variability before the method can become standardized for precise thermodynamic measurements. The discrepancies could be due to experimental uncertainties in balancing the particle at the null point, adverse effects of thermal convection in the cell, and/or unavoidable measurement errors in humidity and temperature.

Because of space limitations, as well as the specific purpose of this review, water activity and density are given only for a few selected inorganic salt systems, most of which are of atmospheric interest. Both water activity and density are expressed in the form of a polynomial in x , the solute wt%, namely,

$$a_1 = 1 + \sum C_i x^i \quad (4.6)$$

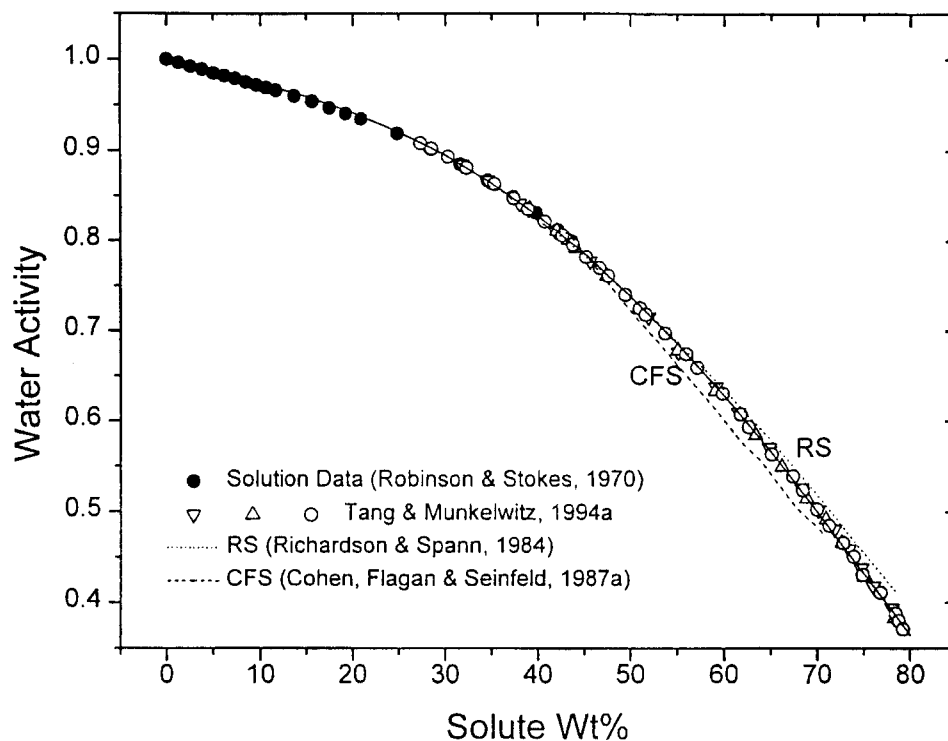


FIGURE 4.6 Water activities of aqueous $(\text{NH}_4)_2\text{SO}_4$ solutions at 25°C.

TA5

Summary of Polynomial Coefficients for Water Activities and Densities

	$(\text{NH}_4)_2\text{SO}_4$	NH_4HSO_4	$(\text{NH}_4)_3\text{H}(\text{SO}_4)_2$	Na_2SO_4		NaHSO_4	NaNO_3	NaCl
x (%)	0-78	0-97	0-78	0-40	40-67*	0-95	0-98	0-48
C_1	-2.715 (-3)	-3.05 (-3)	-2.42 (-3)	-3.55 (-3)	-1.99 (-2)	-4.98 (-3)	-6.366 (-3)	
C_2	3.113 (-5)	-2.94 (-5)	-4.615 (-5)	9.63 (-5)	-1.92 (-5)	3.77 (-6)	1.286 (-4)	8.24 (-5)
C_3	-2.336 (-6)	-4.43 (-7)	-2.83 (-7)	-2.97 (-6)	1.47 (-6)	-6.32 (-7)	-3.496 (-6)	1.158 (-5)
C_4	1.412 (-8)						1.843 (-8)	1.518 (-5)
A_1	5.92 (-3)	5.87 (-3)	5.66 (-3)	8.871 (-3)		7.56 (-3)	6.512 (-3)	7.41 (-3)
A_2	-5.036 (-6)	-1.89 (-6)	2.96 (-6)	3.195 (-5)		2.36 (-5)	3.025 (-5)	-3.741 (-5)
A_3	1.024 (-8)	1.763 (-7)	6.68 (-8)	2.28 (-7)		2.33 (-7)	1.437 (-7)	2.252 (-6)
A_4								-2.06 (-8)

*For this concentration range, $a_w = 1.557 + \sum C_i x_i$.

and

$$\rho = 0.9971 + \sum A_i x_i^i, \quad (4.7)$$

where the polynomial coefficients, C_i and A_i , are given in Table 4.1.

Data for mixed-salt solutions are very limited. Tang et al.^{40,41} measured the water activity of bulk solutions of $(\text{NH}_4)_2\text{SO}_4/\text{NH}_4\text{HSO}_4$ (molar ratio 1/1) and $(\text{NH}_4)_2\text{SO}_4/\text{NH}_4\text{NO}_3$ (3/1; 1/2). Spann and Richardson⁴² measured the water activity of $(\text{NH}_4)_2\text{SO}_4/\text{NH}_4\text{HSO}_4$ ($1.5 \leq [\text{NH}_4^+]/[\text{SO}_4^{2-}] \leq 2$)

TABLE 4.2
Predicted and Observed %RHD for Some Pure-Salt Particles

Salt	Solution Phase	Particle Phase	Pred. %RHD	Obs. %RHD
NaCl	Anhydrous	Anhydrous	75.3	75.3 ± 0.1
KCl	Anhydrous	Anhydrous	84.3	84.2 ± 0.3
(NH ₄) ₂ SO ₄	Anhydrous	Anhydrous	80.0	79.9 ± 0.5
NH ₄ H ₂ SO ₄	Anhydrous	Anhydrous	39.7	40.3 ± 0.5
Na ₂ SO ₄	Decahydrate	Anhydrous	93.6	84.5 ± 0.5
NaNO ₃	Anhydrous	Anhydrous	73.8	74.1 ± 0.5
NH ₄ NO ₃	Anhydrous	Anhydrous	61.8	61.2 ± 0.5
Sr(NO ₃) ₂	Tetrahydrate	amorphous	85	69.1 ± 0.5

solution droplets, using the electrodynamic balance. Cohen et al.⁴³ used the electrodynamic balance to measure the water activity of mixed-electrolyte solution droplets containing NaCl/KCl, NaCl/KBr, or NaCl/(NH₄)₂SO₄. Chan et al.³⁸ used the SVEL to measure the water activity of solution droplets containing various compositions of (NH₄)₂SO₄/NH₄NO₃. Recently, Kim et al.⁶⁴ again used the SVEL to measure the water activity of solution droplets for the (NH₄)₂SO₄/H₂SO₄ system. All investigators seem to agree that the simple empirical relationship, known as the ZSR relation (Zdanovskii,⁴⁴ Stokes and Robinson⁴⁵), is capable of predicting with satisfaction the water activity of mixed-salt solutions up to high concentrations, although other, more elaborate methods may perform better at low concentrations.

For a semi-ideal ternary aqueous solution containing two electrolytes (designated 2 and 3) at a total molality $m = m_2 + m_3$, the ZSR relation

$$\frac{1}{m} = \frac{y_2}{m_{02}} + \frac{y_3}{m_{03}} \quad (4.8)$$

holds when the solution is in isopiestic equilibrium with the binary solutions of the individual electrolyte at respective molalities m_{02} and m_{03} . Here, $y_2 = m_2/m$ and $y_3 = m_3/m$. Semi-ideality refers to the case where the two solutes may interact with the solvent but not with each other. It is also conceivable that a solution behaves semi-ideally when the solute-solute interactions are present but canceling each other. Systems showing departure from semi-ideality are common.⁴⁶ For such systems, a third term, by_2y_3 , can be added to the right-hand side of Equation 4.8, where b is an empirically determined parameter for each system.

PARTICLE DELIQUESCENCE

As discussed earlier, for single-salt particles larger than 0.1 μm, the deliquescence point corresponds to the saturation point of the bulk solution. Thus, %RHD for a single-salt aerosol particle is, in principle, equal to $100a_1^*$, where a_1^* is the water activity of the saturated electrolyte solution. In Table 4.2, the observed %RHD of some inorganic salt particles are compared with predictions from bulk solution data, which are available in the literature (e.g., see References 47 and 48). Note that, within experimental uncertainties, the comparison is reasonably good only for those inorganic salts whose stable crystalline phase in equilibrium with the saturated solution is identical to the observed particle phase.

For a ternary system consisting of two salts as solutes and water as solvent, it is possible to compute the water activity at the eutonic point using the ZSR method. Other estimation methods, such as those by Meissner and Kusik,⁴⁹ Bromly,⁵⁰ and Pitzer⁵¹ are also available in the literature.

TABLE 4.3
Predicted and Observed %RHD for Some Mixed-Salt Particles

System	Eutonic Composition	Solution Phases	Obs. %RHD	Pred. %RHD	
				K-M Method	ZSR Method
KCl(A)	2.183	A + B	72.7 ± 0.3	71.7	72.1
NaCl(B)	5.106				
NaNO ₃ (A)	6.905	A + B	68.0 ± 0.4	65.7	67.1
NaCl(B)	4.161				
Na ₂ SO ₄ (A)	1.057	A · B · 4H ₂ O + B	71.3 ± 0.4	76.4	76.4
(NH ₄) ₂ SO ₄ (B)					
Na ₂ SO ₄ (A)	0.708	A + B	74.2 ± 0.3	75.5	74.7
NaCl(B)	5.530				
Na ₂ SO ₄ (A)	0.413	A · B · 2H ₂ O + B	72.2 ± 0.2	74.6	74.1
NaNO ₃ (B)	10.28				

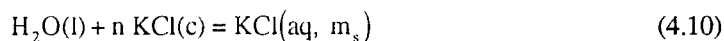
Stelson and Seinfeld⁵² used the M-K method to calculate the water activities for the NH₄NO₃–(NH₄)₂SO₄–H₂O system and found a good agreement between the theoretical predictions and the experimental measurements of Tang et al.⁴¹ Koloutsou-Vakakis and Rood⁵³ also presented a salient description of a thermodynamic model for predicting RHD for the (NH₄)₂SO₄–Na₂SO₄–H₂O system. They compared their %RHD predictions with field measurements by temperature- and humidity-controlled nephelometry, assuming the aerosol sample to be internally mixed.

Table 4.3 shows the comparison of the predicted %RHD by the M-K and ZSR methods with experimental measurements for a number of mixed-salt particles. It is shown that for simple mixed-salt systems, where no crystalline hydrates or double salts are present in the solid phases, the predictions are in good agreement with the measurements. However, for more complicated systems such as the Na₂SO₄–(NH₄)₂SO₄ and the Na₂SO₄–NaNO₃ solutions, where the eutonic composition is in equilibrium with a double salt, the predicted %RHD is somewhat off. Also note that, since in an aerosol particle the solid phase may not be what is expected from the bulk solution, the observed %RHD may also be different from what is predicted on the basis of the bulk-solution eutonic composition.

Klaue and Dannecker^{54,55} investigated the deliquescence properties of the double salts 2NH₄NO₃ · (NH₄)₂SO₄ (2:1) and 3NH₄NO₃ · (NH₄)₂SO₄ (3:1), using a humidity-controlled X-ray diffractometer to observe changes in the crystalline phase. They concluded that %RHD for 2:1 was 68% RHD, instead of 56.4% RH as reported by Tang,³⁴ who made the measurement in a continuous-flow aerosol apparatus. Subsequently, Tang et al.⁴¹ reported water activity measurements for mixed-salt solutions of NH₄NO₃–(NH₄)₂SO₄ and showed that the water activity at the eutonic composition was 0.66, clearly indicating that the earlier measurement was too low. The measurement error could have resulted from water adsorption on aerosol particles due to the presence of NH₄NO₃, which obscured the deliquescence point, just as what might have happened in the case of pure NH₄NO₃ aerosol particles, using the continuous-flow method.

The temperature and composition dependence of the deliquescence humidity has been investigated by Tang and Munkelwitz.^{16,56} Consider, for example, a solid KCl particle surrounded by humid air at a temperature T . At its deliquescence humidity corresponding to a water vapor partial pressure of p_1 atm, the particle transforms into a droplet by condensing, on a molar basis, one mole of water vapor, H₂O(g), onto n moles of crystalline KCl(c) to form a saturated aqueous solution of molality m_v . Assume again the diameter of the droplet to be larger than 0.1 μm so that the Kelvin

effect due to surface tension can be ignored. The vapor-liquid equilibrium can be expressed by the following reactions:



Here, the symbols in the parentheses have the following meanings: *g* denotes vapor, *l* liquid, *c* crystalline, *aq* aqueous solution. The heat that is released in Reaction (4.9) is the heat of condensation of water vapor, which is equal to its heat of vaporization, $-\Delta H_v$. The heat that is absorbed in Reaction (4.10) is the integral heat of solution, ΔH_s , which can be calculated from the heats of formation tabulated in standard thermodynamic tables.²⁶ The overall heat involved in the process is the sum of the two heats:

$$\Delta H = n\Delta H_s - \Delta H_v. \quad (4.11)$$

Thus, applying the Clausius-Clapeyron equation to the phase transformation, one obtains

$$\frac{d \ln p_1}{dT} = -\frac{\Delta H}{RT^2} = \frac{\Delta H_v}{RT^2} - \frac{n\Delta H_s}{RT^2}. \quad (4.12)$$

Since by definition,

$$\frac{d \ln p_1^0}{dT} = \frac{\Delta H_v}{RT^2}, \quad (4.13)$$

it follows that, by combining Equations 4.4, 4.12, and 4.13, one obtains

$$\frac{d \ln a_1}{dT} = -\frac{n\Delta H_s}{RT^2}. \quad (4.14)$$

Here, *n* is the solubility in moles of solute per mole of water, which can be found either in International Critical Tables⁴⁷ or in the compilation by Seidell and Linke.²⁵ For the convenience of integrating Equation 4.14, *n* is expressed as a polynomial in *T*

$$n = A + BT + CT^2. \quad (4.15)$$

Upon substituting *n* from Equation 4.15 into Equation 4.14, rearranging and integrating the resulting equation from a reference temperature, T^* , one obtains

$$\ln \frac{\%RHD(T)}{\%RHD(T^*)} = \frac{\Delta H_s}{R} \left[A \left(\frac{1}{T} - \frac{1}{T^*} \right) - B \ln \frac{T}{T^*} - C(T - T^*) \right]. \quad (4.16)$$

Since for the most electrolyte solutions the thermodynamic properties at 25°C are well documented, 298.2K is a convenient choice for T^* .

The derivation of Equation 4.16 for a single-salt particle is straightforward. Edger and Swan,⁵⁷ in considering the vapor pressure of saturated aqueous solutions, used the Van't Hoff equation

TABLE 4.4
Thermodynamic and Solubility Data of Electrolyte Solutions

Systems	%RHD	ΔH_s (cal mol ⁻¹)	A	B	C
(NH ₄) ₂ SO ₄	79.9 ± 0.5	1510	0.1149	-4.489 (-4)	1.385 (-6)
Na ₂ SO ₄	84.2 ± 0.4	-2330	0.3754	-1.763 (-3)	2.424 (-6)
NaNO ₃	74.3 ± 0.4	3162	0.1868	-1.677 (-3)	5.714 (-6)
NH ₄ NO ₃	61.8	3885	4.298	-3.623 (-2)	7.853 (-5)
KCl	84.2 ± 0.3	3665	-0.2368	1.453 (-3)	-1.238 (-6)
NaCl	75.3 ± 0.1	448	0.1805	-5.310 (-4)	9.965 (-7)

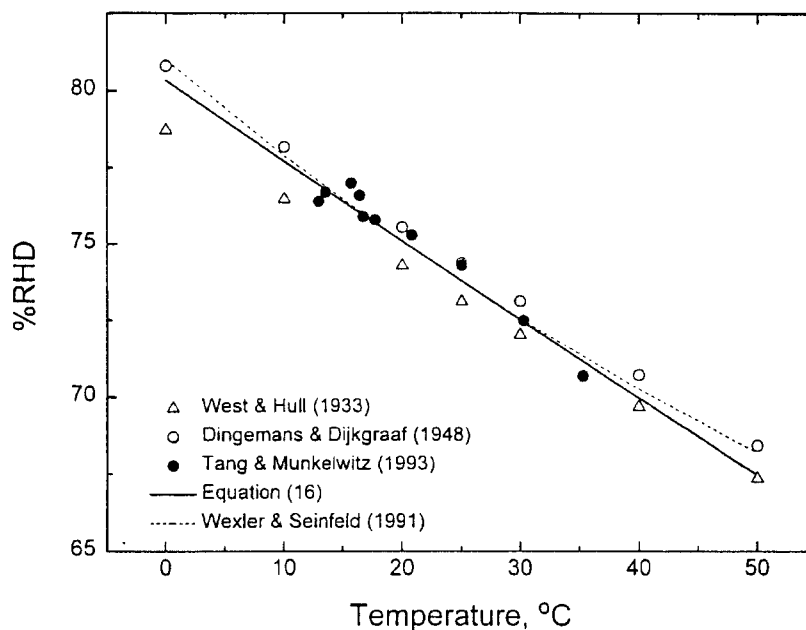


FIGURE 4.7 Deliquescence humidities as a function of temperature for NaNO₃ particles.

relating the solubility to the integral heat of solution and obtained an equation essentially showing that $\ln a_w$ is a linear function of n over a limited temperature increment. Recently, Wexler and Seinfeld³⁰ derived a similar but simplified equation by assuming both constant latent heat and constant saturation molality over a small temperature change. Thus, the derivation of Equation 4.16 here is more rigorous, assuming only that the integral heat of solution is constant.

Equation 4.16 shows that the effect of temperature on %RHD is predominantly governed by the sign and magnitude of the integral heat solution. In Table 4.4, the parameters required for computing %RHD by Equation 4.16 are given for a few inorganic salts of atmospheric interest. Figure 4.7 shows a comparison of %RHD between the bulk solution data (open symbols) and the single-particle measurements (filled circles) for the NaNO₃-H₂O system. A comparison is also shown between characteristics by Equation 4.16 (solid curve) and by a simpler formula (dashed curve) given by Wexler and Seinfeld.³⁰ It is apparent that, while in general the agreement between measurements and theory is good, the single-particle data show less scatter than the bulk-solution data and agree better with theoretical predictions. The two theoretical models also agree with each other in the limited temperature range 10 to 30°C, but start to show some departure at other temperatures as a result of different assumptions used in the solubility data.

For mixed-salt systems, particle deliquescence is determined by the water activity at the eutonic point. Consider, therefore, the deliquescence of a mixed-salt particle at the eutonic composition represented by n_2 moles of NaCl, n_3 moles of KCl and 1 mole of H_2O :



Because of a lack of experimental data for multicomponent systems, the heat that is absorbed in Reaction 4.17 can only be estimated from the respective integral heats of solution for the binary solutions, NaCl– H_2O and KCl– H_2O , namely,

$$\Delta H_s = n_2\Delta H_{s2} + n_3\Delta H_{s3} - \Delta H_1. \quad (4.18)$$

Here, the subscript, 1, refers to the solvent and the other subscript numbers refer to the solutes. The last term in Equation 4.18 accounts for the fact that ΔH_1 , the differential heat of solution due to the solvent, has been included in each of the two integral heats of solution and, therefore, should be subtracted once from the total heat of solution. This is usually a small correction term and can be neglected in most cases.

The solubilities n_2 and n_3 can be obtained from the eutonic composition and expressed as a function of temperature, as in Equation 4.15. Sometimes, polynomials higher than the second order may be needed. Substituting Equation 4.18 into Equation 4.14, rearranging, and integrating lead to the final equation.⁵⁶

$$\begin{aligned} \ln \frac{\%RHD(T)}{\%RHD(T^*)} = & \frac{\Delta H_{s2}}{R} \left[A_2 \left(\frac{1}{T} - \frac{1}{T^*} \right) - B_2 \ln \frac{T}{T^*} - C_2(T - T^*) \right] \\ & + \frac{\Delta H_{s3}}{R} \left[A_3 \left(\frac{1}{T} - \frac{1}{T^*} \right) - B_3 \ln \frac{T}{T^*} - C_3(T - T^*) \right] - \frac{\Delta H_1}{R} \left(\frac{1}{T} - \frac{1}{T^*} \right) \end{aligned} \quad (4.19)$$

Equation 4.19 was derived strictly for the case of simple two-component mixtures forming a single eutonic composition in saturated solutions. Further work is needed for more complex aerosol systems,

Figures 4.8 and 4.9 show, respectively, the results obtained for aerosol particles containing various compositions of KCl–NaCl and $NaNO_3$ –NaCl. The two lines shown for the single-salt particles are computed from theory, using tabulated parameters given in Table 4.4. The corresponding line for mixed-salt particles is computed from Equation 4.19 and pertinent data in Table 4.5. It is clear that the agreement between theory and experiment is good. The slight but noticeable departure at either end of the theoretical line may be due to our assumption of additive heats of solution made in Equation 4.18. Since there is no experimental heat of solution data available for the multicomponent systems of atmospheric interest, Equation 4.19 derived on the basis of additive properties can still be used to provide a reasonable estimate in any ambient aerosol modeling studies, at least in a limited temperature region. It is also worthwhile to point out that, for salt mixtures having simply solubility properties, the deliquescence humidity is governed only by the water activity at the eutonic composition and is thus independent of the initial dry-salt composition. The temperature dependence of the mixed-salt particle usually more or less follows the direction of the component salt whose eutonic solubility is the higher of the two.

As discussed earlier, no simple mathematical analysis is yet possible at the present time for mixed-salt particles containing more than two deliquescent salts. The deliquescence properties of the three-salt system, NaCl– Na_2SO_4 – $NaNO_3$, whose growth curve is shown in Figure 4.4, was

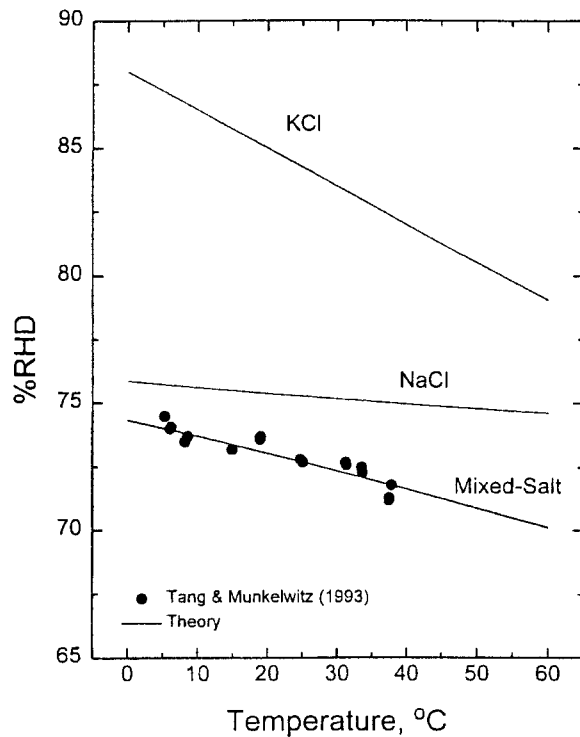


FIGURE 4.8 Deliquescences humidities as a function of temperature for mixed KCl-NaCl particles.

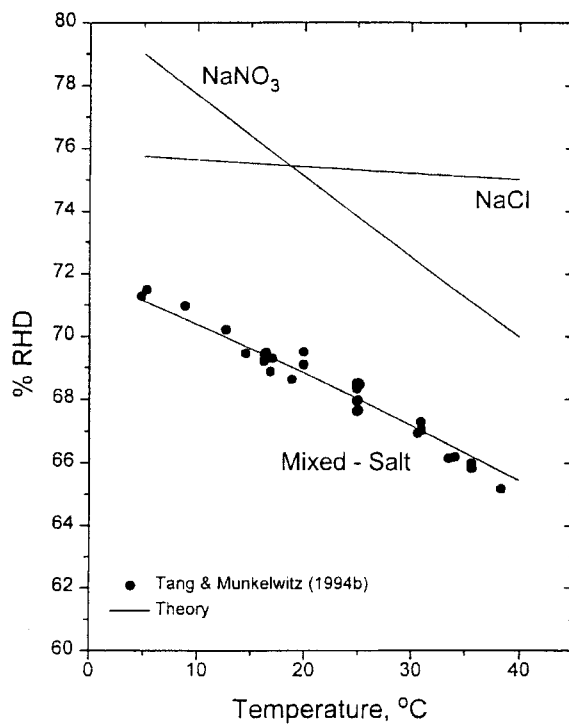


FIGURE 4.9 Deliquescence humidities as a function of temperature for mixed Na_2SO_4 - NaNO_3 particles.

TABLE 4.5
Thermodynamic and Solubility Data of Aqueous Mixed-Salt Solutions

System	%RHD at T^*	Δh_u (cal mol ⁻¹)	A_i	B_i	C_i	D_i
NaCl	72.7 ± 0.3	448	2.618 (-1)	-9.412 (-4)	1.254 (-6)	
KCl		3665	-6.701 (-2)	1.394 (-4)	7.225 (-7)	
Na ₂ SO ₄	72.2 ± 0.2	-2330	-4.591	4.413 (-2)	-1.407 (-4)	1.489 (-7)
NaNO ₃		3162	6.134	-5.847 (-2)	1.852 (-4)	1.879 (-7)
(NH ₄) ₂ SO ₄	71.3 ± 0.4	1510	1.977 (-2)	2.617 (-4)		
Na ₂ SO ₄		-2330	-2.187	2.343 (-2)	-8.411 (-5)	1.017 (-7)
NaCl	68.0 ± 0.4	448	5.957 (-1)	-3.745 (-3)	9.134 (-6)	-8.173 (-9)
NaNO ₃		3162	4.532 (-1)	-4.106 (-3)	9.909 (-6)	5.552 (-10)
NaCl	74.2 ± 0.3	448	-5.313 (-1)	5.477 (-3)	-1.631 (-5)	1.689 (-8)
Na ₂ SO ₄		-2330	-4.584 (-1)	5.000 (-3)	-1.723 (-5)	1.933 (-8)

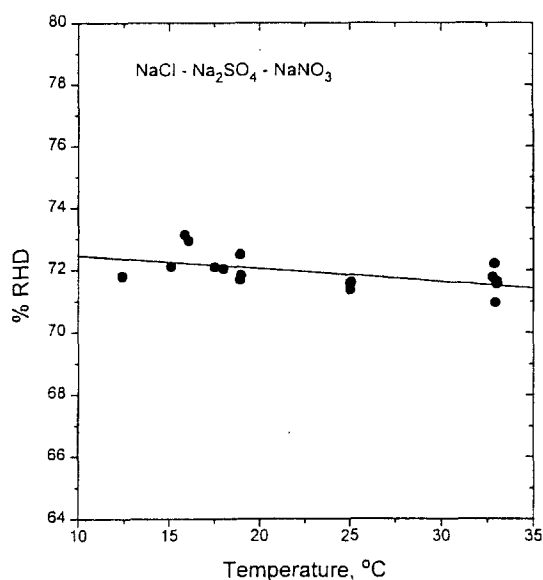


FIGURE 4.10 Deliquescence humidities as a function of temperature for mixed Na₂SO₄-NaNO₃-NaCl particles.

studied in the limited temperature range 12 to 33°C. The results shown in Figure 4.10 indicate that, within experimental error, the deliquescence humidity can be considered constant at 71.8 ± 0.5%. A least-squares line drawn through the data points shows only very slightly, if any, temperature dependence. Because ambient aerosols are likely multicomponent systems composed of more than two inorganic salts, further work to elucidate the hygroscopic properties of these complex aerosols is needed in order to predict their transport and light-scattering behavior in a humid environment.

SOLUTE NUCLEATION AND DROPLET EFFLORESCENCE

The persistence of a solution drop during evaporation to high degrees of supersaturation with respect to the solute is typical of suspended hygroscopic aerosol particles, which are free of the presence of foreign substrates. While the droplet is in equilibrium with the surrounding water vapor, it is metastable with respect to the solid-phase solute. Therefore, solute nucleation is expected: the

higher the degree of supersaturation, the larger the nucleation rate.⁵⁸ According to the classical nucleation theory, the net rate of embryo formation, J , per unit volume per unit time is given by

$$J = K \exp(-\Delta G_c/kT), \quad (4.20)$$

where ΔG_c is the maximum free-energy barrier to transition to the more stable phase and k the Boltzmann constant. K , an undetermined kinetic factor, is either estimated from the binary collision frequency to the reaction rate theory⁵⁹ or expressed by some complex formula derived from various theories as discussed by Tamara et al.⁶⁰ Theoretical estimates of its value range from 10^{24} to 10^{36} $\text{cm}^{-3} \text{s}^{-1}$. An intermediate value that has been commonly used is $10^{30} \text{cm}^{-3} \text{s}^{-1}$. For a given rate of critical nucleus formation, J , the expected induction time, t_i , before a nucleation event happens in a droplet of volume, V_d , is given by⁶¹

$$t_i = \frac{1}{V_d J}. \quad (4.21)$$

Substituting Equation 4.21 into Equation 4.20 and rearranging, one obtains

$$\Delta G_c = kT \ln(V_d t_i K). \quad (4.22)$$

Assume that the nucleation embryos are crystallites formed by density fluctuations in the supersaturated solution droplet. The free-energy barrier to nucleation of a given-size crystalline embryo is

$$\Delta G = A\sigma + V\Delta G_v, \quad (4.23)$$

where A and V are, respectively, the total interfacial area and volume of the embryo, σ is the average interfacial free energy based on A , and ΔG_v is the excess free energy per unit volume of the embryo over that of the solution. For simplicity, the embryo is usually assumed to be spherical in shape so that A and V can be expressed in term of its radius, r . Other shapes consistent with the unit cells specific to given crystalline habits have also been considered, using an appropriately defined characteristic length.^{14,62,63}

If the solute in the saturated solution is chosen as the references state and the definition of the solute mean activities is invoked, then, ΔG_v is given by

$$\Delta G_v = -\frac{v\rho_0 RT}{M} \ln \frac{a_{\pm}}{a_{\pm}^*}, \quad (4.24)$$

where a_{\pm} and a_{\pm}^* are, respectively, the solute mean activities in the supersaturated and saturated solutions. M is the solute molecular weight, ρ_0 is the density of the crystalline phase, and v is the number of ions produced by the dissociation of a salt molecule.

The critical size of the embryo corresponding to the maximum free-energy barrier is obtained, in the case of a spherical embryo, by letting $(\partial\Delta G/\partial r) = 0$. Hence,⁶³

$$r_c = -\frac{2\sigma}{\Delta G_v} \quad (4.25)$$

TABLE 4.6
Properties of Nucleation Embryos in Aqueous Salt Solutions

Salt	m (critical)	S (critical)	σ (ergs cm ²)	r (critical)	N (# molecules)
NaCl	13.8 ^a	5.15 ^a	104	6.81	30
	13	5.23	103	6.84	30
KCl	12.3 ^a	3.64 ^a	70.4	8.26	38
	12.6 ^b	3.4 ^b	67.9	8.41	40
	12.5	2.91	62.0	8.81	46
(NH ₄) ₂ SO ₄	17.5 ^a	2.52 ^a	46.6	10.2	35
	30	3.05	52.8	9.55	29
Na ₂ SO ₄	13.2 ^a	3.71 ^a	74.1	8.06	25
	14	2.7	61.6	8.83	33
NaNO ₃	78	2.97	62.9	8.74	45
	380	3.45	68.5	8.38	39

^a footnote??

^b footnote??

and, consequently,

$$\sigma^3 = \frac{3kT \ln(V_d t_i K)}{16\pi} \left[\frac{v p_0 RT}{M} \ln S_{\pm} \right]^2, \quad (4.26)$$

where S_{\pm} is the critical supersaturation at the onset of crystallization and is given by the ratio, a_{\pm}/a_{\pm}^* . Using the Gibbs-Duhem equation, $\ln S_{\pm}$ can be calculated from the water activity measurement according to the following equation⁴⁵:

$$\ln S_{\pm} = \int_{a_1^*}^{a_1} \frac{55.51}{vm} d \ln a_1. \quad (4.27)$$

Here, $\ln a_1$ is usually expressed as a polynomial in solute molality for the convenience of carrying out the integration.

In droplet crystallization experiments, S_{\pm} can be measured with much higher precision than what would be possible in bulk solution studies. Thus, the uncertainties in σ determination by the single-particle levitation experiment lie largely in estimating the product $(V_d t_i K)$. Taking a typical droplet of 15 μm in diameter, an induction time about 1 s, and 10^{30} for K , the estimate of $\ln(V_d t_i K)$ is about 49, a representative value for ionic solution droplets. A change in the product by two orders of magnitude results in about 3% change in the value of σ , whereas a 15% change in S would lead to about 7% change in σ .

In Table 4.6, the estimated interfacial energy, σ , critical embryo size, r_c , and number of molecules, N , in the spherical embryo are given for some common inorganic salts. The calculation is based on the solute concentration in molality, m , and supersaturation, S , measured at the onset of solute nucleation in droplets. It is worthwhile to note that, although for each system there are discrepancies in the observed critical supersaturations, the estimated embryo properties show reasonable agreement. In addition, the nucleation embryo properties for NaNO₃, a highly hygroscopic salt, do not vary much, despite the fact that the critical solute concentration may span a

wide range from 78 to 380 m. The invariance appears to give credence to the embryo properties determined from studies of homogeneous nucleation in suspended aqueous solution droplets.

ACKNOWLEDGMENT

The author is indebted to his colleague, Harry R. Munkelwitz, who designed and constructed the single-particle levitation apparatus and performed the experiments reported through the years. This research was performed under the auspices of the U.S. Department of Energy under Contract No. DE-AC02-98CH10886.

REFERENCES

1. La Mer, V.K. and Gruen, R., *Trans. Faraday Soc.*, 48, 410, 1952.
2. Junge, C.E., *Ann. Met.*, 5, 1, 1952.
3. Winkler, P., *J. Aerosol Sci.*, 4, 373, 1973.
4. Tang, I.N., *J. Aerosol Sci.*, 7, 361, 1976.
5. Dessens, H., *Q. J. R. Meteor. Soc.*, 75, 23, 1949.
6. Twomey, S., *J. Meteor.*, 11, 334, 1954.
7. Orr, C. Jr., Hurd, F.K., and Corbett, W.J., *J. Colloid Sci.*, 13, 472, 1958.
8. Winkler, P. and Junge, C.E., *J. Rech. Atm.*, 6, 617, 1972.
9. Covert, D.S., Charlson, R.J., and Ahlquist, N.C., *J. Appl. Meteor.*, 11, 968, 1972.
10. Tang, I.N. and Munkelwitz, H.R., *J. Aerosol Sci.*, 8, 321, 1977.
11. Davis, E.J., *Aerosol Sci. Technol.*, 2, 121, 1983.
12. Richardson, C.B. and Spann, J.F., *J. Aerosol Sci.*, 15, 563, 1984.
13. Tang, I.N., Munkelwitz, H.R., and Wang, N., *J. Colloid Interface Sci.*, 14, 409, 1986.
14. Cohn, M.D., Flagan, R.C., and Seinfeld, J.H., *J. Phys. Chem.*, 91, 4563, 1987a.
15. Tang, I.N. and Munkelwitz, H.R., *Aerosol Sci. Technol.*, 15, 201, 1991.
16. Tang, I.N. and Munkelwitz, H.R., *J. Geophys. Res.*, 99, 18801, 1994a.
17. Davis, E.J., *Advances in Chemical Engineering*, Vol. 18, Academic Press, San Diego, 1992.
18. Richardson, C.B. and Kurtz, C.A., *J. Am. Chem. Soc.*, 106, 6615, 1984.
19. Straubel, H., *Z. Elektrochem.*, 60, 1033, 1956.
20. Wueker, R.F., Shelton, H., and Langmuir, R.V., *J. Appl. Phys.*, 30, 342, 1959.
21. Frickel, R.B., Shaffer, R.E., and Stamatoff, J.B., *Chambers for the Electrodynamic Containment of Charged Particles*, U.S. Department of Commerce, National Technical Information Service, Report #AD/A056 236, 1978.
22. Davis, E.J., *Langmuir*, 1, 379, 1985.
23. Rood, M.J., Shaw, M.A., Larson, T.V., and Covert, D.S., *Nature*, 337, 537, 1989.
24. Tang, I.N., Fung, K.H., Imre, D.G., and Munkelwitz, H.R., *Aerosol Sci. Technol.*, in press, 1995.
25. Seidell, A. and Linke, W.F., *Solubilities of Inorganic and Metal Organic Compounds*, 4th ed., *Am. Chem. Soc.*, Washington, D.C. 1965.
26. Wagman, D.D., Evans, W.H., Halow, I., Parker, V.B., Bailey, S.M., and Schumm, R.H., *Selected Values of Chemical Thermodynamic Properties*, National Bureau of Standards Technical Note 270, U.S. Department of Commerce, Washington, D.C., 1966.
27. Goldberg, R.N., *J. Phys. Chem. Ref. Data*, 10, 671, 1981.
28. Tang, I.N. and Munkelwitz, H.R., *J. Appl. Meteor.*, 33, 791, 1994b.
29. Kirgintsev, A.N. and Trushnikova, L.N., *Russ. J. Inorg. Chem.*, 13, 600, 1968.
30. Wexler, A.S. and Seinfeld, J.H., *Atmos. Environ.*, 25A, 2731, 1991.
31. Koehler, H., *Trans. Faraday Soc.*, 32, 1152, 1936.
32. Dufour, L. and Defay, R., *Thermodynamic of Clouds*, Academic Press, New York, 1963.
33. Pruppacher, H.R. and Klett, J.D., *Microphysics of Cloud and Precipitation*, D. Reidel, Dordrecht, Holland, 1978.
34. Tang, I.N., *Generation of Aerosols*, Willeke, K. Ed., Chap. 7, Ann Arbor Sci., Ann Arbor, MI, 1980.

35. Clegg, S.L. and Pitzer, K.S., *J. Phys. Chem.*, 96, 3513, 1992.
36. Clegg, S.L., Pitzer, K.S., and Brimblecombe, P., *J. Phys. Chem.*, 96, 9470, 1992.
37. Clegg, S.L. and Brimblecombe, P., *J. Aerosol Sci.*, 26, 19, 1995.
38. Chan, C.K., Flagan, R.C., and Seinfeld, J.H., *Atmos. Environ.*, 26A, 1661, 1992.
39. Arnold, S. and Folan, L.M., *Rev. Sci. Instr.*, 58, 1732, 1987.
40. Tang, I.N., Munkelwitz, H.R., and Davis, J.G., *J. Aerosol Sci.*, 9, 505, 1978.
41. Tang, I.N., Wong, W.T., and Munkelwitz, H.R., *Atmos. Environ.*, 15, 2463, 1981.
42. Spann, J.F. and Richardson, C.B., *Atmos. Environ.*, 19, 819, 1985.
43. Cohn, M.D., Flagan, R.C., and Seinfeld, J.H., *J. Phys. Chem.*, 91, 4575, 1987b.
44. Zdanovskii, A.B., *Trudy Solyanoi Laboratorii Akad. Nauk SSSR*, No., 6, 1936.
45. Stokes, R.A. and Robinson, R.H., *J. Phys. Chem.*, 70, 2126, 1966.
46. Sanster, J. and Lenzi, F., *Can. J. Chem. Eng.*, 52, 392, 1974.
47. West, C.J. and Hull, C., *International Critical Tables*, McGraw-Hill, New York, 1933.
48. Robinson, R.A. and Stokes, R.H., *Electrolyte Solutions*, Butterworth, London, 1970.
49. Meissner, H.P. and Kusik, C.L., *AIChE J.*, 18, 294, 1972.
50. Bromley, L.A., *AIChE J.*, 19, 313, 1973.
51. Pitzer, K.S., *J. Phys. Chem.*, 77, 268, 1973.
52. Stelson, A.W. and Seinfeld, J.H., *Atmos. Environ.*, 16, 2507, 1982.
53. Koloutsou-Vakakis, S. and Rood, M.J., *Tellus*, 46B, 1, 1994.
54. Klaue, B. and Dannecker, W., *J. Aerosol Sci.*, 25, S189, 1993.
55. Klaue, B. and Dannecker, W., *J. Aerosol Sci.*, 25, S287, 1994.
56. Tang, I.N. and Munkelwitz, H.R., *Atmos. Environ.*, 27A, 467-473, 1993.
57. Edger, G. and Swan, W.O., *J. Am. Chem. Soc.*, 44, 570, 1992.
58. Walton, A.G., *The Formation and Properties of Precipitates*, Interscience, New York, 1967.
59. Turnbull, D. and Fisher, J.C., *J. Chem. Phys.*, 17, 71, 1949.
60. Tamara, D., Snyder, T.D., and Richardson, C.B., *Langmuir*, 9, 347, 1993.
61. Cohn, M.D., Flagan, R.C., and Seinfeld, J.H., *J. Phys. Chem.*, 91, 4583, 1987c.
62. Enustun, B.V. and Turkevich, J., *J. Am. Chem. Soc.*, 82, 4502, 1960.
63. Tang, I.N. and Munkelwitz, H.R., *J. Colloid Interface Sci.*, 98, 430, 1984.
64. Kim, Y.P., Pun, B.K.-L., Chan, C.K., Flagan, R.C., and Seinfeld, J.H., *Aerosol Sci. Technol.*, 20, 275, 1994.
65. Dingemans, P. and Dijkgraaf, L.L., *Rec. Trav. Chim.*, 67, 231, 1948.